

# Secure Communication of UAV-mounted STAR-RIS under Phase Shift Errors

Aseel Qsibat, Habiba Akhleifa, Abdelhamid Salem, Khaled Rabie, *Senior Member, IEEE*, Xingwang Li, *Senior Member, IEEE*, Thokozani Shongwe, Mohamad A. Alawad, and Yazeed Alkhrijah

**Abstract**—This paper investigates the secure communication capabilities of a non-orthogonal multiple access (NOMA) network supported by a STAR-RIS (simultaneously transmitting and reflecting reconfigurable intelligent surface) deployed on an unmanned aerial vehicle (UAV), in the presence of passive eavesdroppers. The STAR-RIS facilitates concurrent signal reflection and transmission, allowing multiple legitimate users—grouped via NOMA—to be served efficiently, thereby improving spectral utilization. Each user contends with an associated eavesdropper, creating a stringent security scenario. Under Nakagami fading conditions and accounting for phase shift inaccuracies in the STAR-RIS, closed-form expressions for the ergodic secrecy rates of users in both transmission and reflection paths are derived. An optimization framework is then developed to jointly adjust the UAV’s positioning and the STAR-RIS power splitting coefficient, aiming to maximize the system’s secrecy rate. The proposed approach enhances secure transmission in STAR-RIS-NOMA configurations under realistic hardware constraints and offers valuable guidance for the design of future 6G wireless networks.

**Index Terms**—STAR-RIS, NOMA, UAV, physical layer security, phase estimation errors, weighted sum secrecy rate, ergodic capacity.

## I. INTRODUCTION

WITH the global rollout of fifth-generation (5G) wireless networks, researchers are now focusing on the development of next-generation communication systems, namely, sixth-generation (6G) networks. These advancements aim to meet increasingly stringent demands, including enhanced spectral efficiency, improved energy efficiency (EE), ultra-low

latency, and expanded coverage [1] all to ensure the desired quality of service (QoS).

Among others, the advent of reconfigurable intelligent surfaces (RIS) has introduced a revolutionary technology for augmenting spectral and energy efficiency [2]. RIS is made up of a flat array of inexpensive passive components, where each element can control electromagnetic (EM) waves by adjusting their phase shifts using built-in PIN diodes [3]. By dynamically tuning these phase shifts via an intelligent controller, the RIS can enhance signal strength at intended receivers while suppressing interference or signals directed toward eavesdroppers. Unlike traditional techniques—such as artificial noise injection [4] or multi-antenna beamforming [5]—RIS operates passively without requiring additional RF chains, making it both energy-efficient and cost-effective. Moreover, RIS can be seamlessly integrated into existing infrastructure by mounting it on surfaces like building facades, windows, or even clothing, offering flexible deployment options [6].

However, conventional RIS technology only reflects incoming signals, restricting communication to one side of the surface (the reflection plane) [7]. Early investigations into the practical realization of metasurfaces capable of both transmission and reflection were presented in [8]. Building on these findings, the adoption of STAR-RIS in wireless communication has shown practical potential, though it introduces a complex and adversarial operating environment. In contrast to conventional RIS technology, STAR-RIS is capable of independently adjusting both the transmission and reflection coefficients at each element. This capability allows a single transmitter to simultaneously serve users located on both sides of the RIS, effectively enabling 360-degree coverage and overcoming the directional limitations of traditional RIS systems [7]. Numerous studies have explored the performance improvements offered by RIS in various communication contexts. For example, [9] developed a low-complexity strategy for managing the trade-off between sum-rate and energy usage in a RIS-enhanced NOMA system, employing the successive convex approximation (SCA) technique to alternately handle beamforming and phase shift optimization. In a separate study, the authors in [10] focused on improving the long-term energy efficiency (EE) of STAR-RIS-enabled CoMP networks by jointly optimizing active and passive beamforming, incorporating fractional programming and deep reinforcement learning (DRL) to determine an adaptive, near-optimal solution. Moreover, both perfect and imperfect RIS conditions were explored in [11], within CoMP scenarios, where optimal reflection parameters were determined using a dual Lagrangian

Corresponding authors: A. Salem and Mohamad A. Alawad.

Aseel Qsibat and Habiba Akhleifa are with the Department of Electronic and Electrical Engineering, Benghazi University, Benghazi 1308, Libya, (e-mails: aseelqsibat@gmail.com, habiba.akhleifa@gmail.com).

A. Salem is with the Department of Electronic and Electrical Engineering, University College London, London, UK, (e-mail: a.salem@ucl.ac.uk). A. Salem is also affiliated with the Department of Electronic and Electrical Engineering, Benghazi University, Benghazi 1308, Libya.

Khaled Rabie is with the Department of Computer Engineering, King Fahd University of Petroleum and Minerals (KFUPM), Dhahran, Saudi Arabia (email: k.rabie@kfupm.edu.sa).

X. Li is with the School of Physics and Electronic Information Engineering, Henan Polytechnic University, Jiaozuo 454003, China, and also with National Mobile Communications Research Laboratory, Southeast University, Nanjing 210096, China (e-mail: lixingwangbupt@gmail.com).

Thokozani Shongwe is with the Department of Electrical and Electronic Engineering Technology, University of Johannesburg, South Africa.

Mohamad A. Alawad is with the Department of Electrical Engineering, Imam Mohammad Ibn Saud Islamic University (IMSIU), Riyadh, Saudi Arabia, (email: maaawaad@imamu.edu.sa).

Yazeed Alkhrijah is with the Department of Electrical Engineering, College of Engineering, Imam Mohammad Ibn Saud Islamic University (IMSIU), Riyadh, Saudi Arabia, (email: ymalkhrijah@imamu.edu.sa).

framework. In [12], analyzed the performance enhancement of RIS in semi-grant-free NOMA systems, proposing customized algorithms tailored to various RIS configurations. Furthermore, the authors in [13] addressed the sum-rate maximization problem in a multi-UAV NOMA network by jointly optimizing UAV deployment, transmit power, RIS reflection matrix, and NOMA decoding order. To efficiently solve this complex problem, a block coordinate descent (BCD)-based iterative algorithm was developed. Additionally, [14] proposed an innovative distributionally robust reinforcement learning (DRRL) approach, which simultaneously optimizes the UAV's flight path, the active beamforming at the UAV, and the passive beamforming at the STAR-RIS. This integrated design aims to improve the performance of UAV communication systems supported by STAR-RIS. Meanwhile, UAVs have emerged as crucial enablers for future wireless networks due to their cost-effectiveness, rapid deployment, and mobility [15], serving as aerial base stations, relays, or wireless chargers to enhance coverage and capacity [16]. Recent advances combine UAVs with RIS, creating mobile RIS platforms that offer dynamic beamforming capabilities [17]. This integration appears in two primary configurations: ground-based RIS assisting UAV-ground communications [18], [19] and aerial RIS mounted on UAVs for omnidirectional coverage [16]. While UAV-mounted RIS provides deployment flexibility and improved LoS connectivity [20], it introduces complex co-design challenges for RIS configuration and UAV positioning. These hybrid systems present new opportunities to enhance both coverage and security in next-generation networks, though practical implementation hurdles remain regarding real-time optimization of RIS parameters and UAV trajectory planning in dynamic environments. At this point, the role of physical layer security (PLS) becomes crucial in addressing these challenges by leveraging the inherent characteristics of the wireless medium to provide low-complexity and real-time adaptable security solutions.

The PLS enhances data confidentiality by exploiting the inherent randomness of wireless channels, complementing traditional cryptographic methods [21]. Integrating RIS into PLS frameworks introduces several key benefits. In particular, RIS enables passive beamforming through its passive elements, allowing precise control over signal propagation and resulting in significant improvements in secrecy performance [22]. Additionally, RIS can provide signal coverage in environments where direct links are obstructed [23], making it especially suitable for deployment near legitimate users in blocked or non-line-of-sight (NLoS) scenarios. Its compatibility with existing infrastructure further reduces deployment costs and complexity [24]. In this context, [25] analyzed the secrecy rate maximization of an RIS-assisted multi-antenna system under constraints of transmission power and RIS phase shifts. Building on this, [26] proposed a power-efficient secure transmission design. The work in [27], investigated the joint use of RIS and artificial noise (AN) to further enhance PLS. Moreover, [28] explored the application of RIS in device-to-device and relay-based systems, demonstrating its effectiveness in improving secrecy performance across diverse communication scenarios.

Several studies have examined the potential of RIS-assisted secure communication systems, leveraging a combination of active transmit and passive reflective beamforming along with various optimization techniques to enhance the secrecy rate. For instance, in [29], the authors investigated the secrecy performance of RIS-assisted mmWave/THz communication systems by jointly designing transmit beamforming and discrete phase shifts to maximize the secrecy rate. In [30], the impact of hardware impairments was considered in the context of RIS-aided PLS networks with multi-antenna transmitters. Expanding on this, [31] analyzed a secure communication scenario involving multiple multi-antenna eavesdroppers and a NLoS channel between the access point and the legitimate user. Collectively, these works highlight the effectiveness of RIS in strengthening physical layer security while maintaining energy efficiency. Furthermore, they suggest that uniformly distributing the reflecting elements across multiple RIS units is a promising strategy for boosting PLS and harnessing macro-diversity gains.

The deployment of flying RIS is typically constrained to ensure that both the transmitter and receiver remain on the same side of the surface, which inherently limits the achievable system performance. To address this limitation, STAR-RIS has been introduced to enable full-space coverage. STAR-RIS achieves this by concurrently reflecting and transmitting incident signals toward both the same-side and opposite-side half-spaces relative to the source node, as demonstrated in [32], [33]. Furthermore, STAR-RIS and NOMA exhibit a mutually beneficial relationship—STAR-RIS can significantly expand the coverage area of NOMA systems, while NOMA can enhance the overall spectral efficiency and user access capabilities of STAR-RIS-assisted networks [34], [35], [36]. However, despite the transformative potential of STAR-RIS, especially when deployed on UAV platforms, the PLS performance of such systems remains largely unexplored. This critical research gap is further exacerbated by real-world challenges—most notably, the phase distortion caused by UAV vibrations and aerodynamic turbulence, which introduces non-negligible phase estimation errors that degrade beamforming accuracy and secrecy performance.

Motivated by this, in this work, we conduct a detailed performance evaluation of a UAV-enabled communication system incorporating a STAR-RIS. By harnessing the UAV's mobility alongside the STAR-RIS's full-space signal manipulation capability, we aim to boost the secrecy performance of NOMA networks—particularly in scenarios affected by phase estimation errors resulting from UAV instability and airflow fluctuations. We also explore optimal strategies for power allocation and the placement of both the UAV and STAR-RIS in environments involving multiple legitimate users and eavesdroppers.

The main contributions of this paper are summarized as follows:

- We investigate a UAV-mounted STAR-RIS-assisted downlink NOMA communication system in the presence of multiple eavesdroppers. To fully exploit the 360-degree transmission and reflection capability of the STAR-RIS, a user pairing strategy is proposed to serve users located in

## II. SYSTEM MODEL

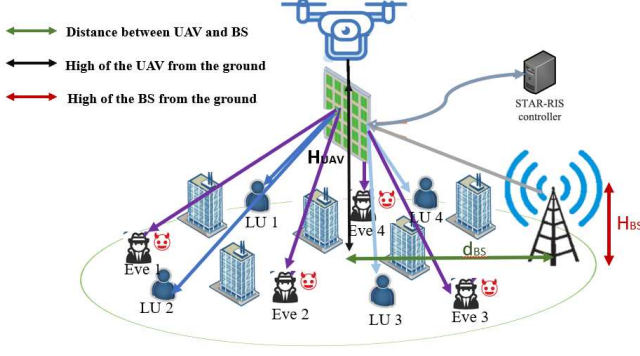


Figure 1. UAV-mounted STAR-RIS-assisted Secure Downlink NOMA Communications System

both the reflection and transmission regions via NOMA. Under this framework, we derive closed-form expressions for the ergodic secrecy rates of legitimate users in both regions.

- To realistically account for channel impairments caused by UAV mobility, we model the phase estimation errors using a von Mises distribution, which captures practical distortions such as jittering and airflow. Leveraging this model, we analytically derive ergodic secrecy rate expressions that are computationally efficient and provide results consistent with Monte Carlo simulations.
- To enhance the PLS performance, we formulate a joint optimization problem to maximize the Weighted Sum Secrecy Rate (WSSR) by simultaneously optimizing the UAV's 3D hovering position and transmit power allocation among NOMA users.
- Due to the non-convex nature of the formulated problem, we decompose this problem into two subproblems: one for UAV positioning and the other for power allocation. An iterative alternating optimization algorithm is proposed to solve the problem efficiently until convergence.
- Specifically, the 3D UAV position is optimized using a linear grid-based search over a discretized space to find the best hovering location, while the power allocation is optimized using a global search algorithm, which is well-suited for handling the highly non-convex and continuous nature of the power control problem in NOMA systems with secrecy constraints.

The remainder of this paper is organized as follows. Section II outlines the system model and formulates the joint optimization framework for a UAV-assisted STAR-RIS downlink NOMA system under a fixed deployment scenario. Section III describes the proposed algorithms developed to address this optimization task. Section V presents simulation results that validate the efficiency of the proposed solutions and demonstrate the benefits of integrating STAR-RIS with UAVs. Lastly, Section VI provides concluding remarks.

As illustrated in Fig. 1, we consider a secure downlink transmission scenario in a NOMA system assisted by a UAV-mounted STAR-RIS. A ground base station (BS) communicates with multiple single-antenna legitimate users (LUs), which are divided into two distinct groups: the legitimate users are positioned within both the reflection and transmission regions of the STAR-RIS. Considering the presence of eavesdroppers (Eves) distributed across both sides of the STAR-RIS, it is assumed that the direct communication links between the base station (BS) and the users are obstructed by environmental barriers. This assumption reflects a widely adopted worst-case scenario in physical layer security (PLS) analyses. [34].

Let the number of legitimate users be denoted by  $K = K_r + K_t$ , where  $K_r$  and  $K_t$  represent the number of users in the reflection and transmission regions, respectively. Similarly, let  $E$  be the number of single-antenna eavesdroppers and  $M$  be the number of elements on the STAR-RIS. The STAR-RIS, mounted on a UAV, is capable of adjusting its position and altitude dynamically, allowing for more adaptable line-of-sight (LoS) connectivity with ground users while improving the system's spatial responsiveness. [37].

We adopt a NOMA scheme in which each time-frequency resource block is shared by a user pair—one from the reflection region and one from the transmission region. Power allocation is asymmetric: the reflect-region user, typically closer to the UAV, is allocated less power, while the transmit-region user, being further, receives more power but is subject to stronger interference. This pairing strategy aligns with established NOMA protocols, which leverage successive interference cancellation (SIC) for decoding [38], that can be viewed as the worst-case scenario<sup>1</sup>. In this paper, a 3D Cartesian coordinate system is adopted. The horizontal locations of LU  $k \in \mathcal{K}$  and Eve  $e \in \mathcal{E}$  are denoted by  $C_k = [x_k, y_k, z_k]$  and  $C_e = [x_e, y_e, z_e]$ , respectively. Moreover, the location of the UAV is denoted by  $C_u = [x_u, y_u, z_u]$ .

All wireless channels are modeled using Nakagami- $m$  fading, which provides a flexible and generalized fading framework appropriate for various propagation conditions. To account for practical impairments in STAR-RIS implementation, phase errors introduced by the STAR-RIS elements are modeled as von Mises-distributed random variables, capturing the imperfections in phase control due to hardware limitations [39].

In the context of the STAR-RIS, the transmission coefficient (TCs) and reflection coefficient (RCs) matrices are denoted as  $\Theta_t \in \mathbb{C}^{M \times M}$  and  $\Theta_r \in \mathbb{C}^{M \times M}$ , respectively. Correspondingly, we have  $\Theta_t = \text{diag} \left\{ \sqrt{\zeta_t^1} e^{-j\theta_t^1}, \dots, \sqrt{\zeta_t^M} e^{-j\theta_t^M} \right\}$  and  $\Theta_r = \text{diag} \left\{ \sqrt{\zeta_r^1} e^{-j\theta_r^1}, \dots, \sqrt{\zeta_r^M} e^{-j\theta_r^M} \right\}$ , where  $\zeta_q^m \in [0, 1]$  and  $\theta_q^m \in [0, 2\pi)$ ,  $q \in [r, t]$  are the amplitude and phase shift of element  $m$ , respectively. Similar to [40], the UAV-mounted STAR-RIS communicates with the controller through wireless

<sup>1</sup>Note that the assumption of single-antenna eavesdroppers represents a fundamental baseline threat model, while scenarios involving multi-antenna eavesdroppers will be studied in our future works.

backhaul links, which are used to configure its transmission and reflection coefficients. Specifically, the amplitudes  $\zeta_t^m$  and  $\zeta_r^m$  are coupled to satisfy the conditions of  $\zeta_t^m + \zeta_r^m = 1$  due to the law of energy conservation, while the phase shifts  $\vartheta_t^m$   $\vartheta_r^m$  can be independently adjusted. Similar to [36], it is assumed that the direct links between the legitimate users (LUs) and the base station (BS) are obstructed by environmental obstacles, representing one of the most challenging conditions for conventional communication systems. Furthermore, it is assumed that the UAV has access to the location information of each legitimate user (LU) and eavesdropper (Eve) through the use of on-board optical cameras or synthetic aperture radar. [41].

### A. Signal Model

In the considered STAR-RIS-assisted UAV communication system, NOMA is employed to enhance spectral efficiency by allowing simultaneous transmission to multiple users over the same frequency band. In this framework, the BS transmits a superimposed signal composed of different user messages, each assigned a distinct power level based on their channel conditions. Specifically, the BS allocates a portion of its total transmit power  $P_s$  to serve users in both the reflection and transmission regions of the STAR-RIS. The transmitted signal is given by:

$$S = \sqrt{\rho P_s} x_r + \sqrt{(1-\rho)P_s} x_t, \quad (1)$$

where  $x_r$  and  $x_t$  present the information signals intended for users in the reflection and transmission regions, respectively, using power-domain NOMA  $\rho \in [0, 1]$ .

The cascaded channels from the BS to a user (or eavesdropper) involve the links from BS to STAR-RIS and STAR-RIS to receiver.  $h_i$  and  $\{g_{k_{q_i}}/g_{e_{q_i}}\}$  represent the channel from the BS to the RIS and the channel from the ground RIS to LUs/Eves, where  $q \in [r, t]$ . Therefore, after applying SIC, the received signal at the legitimate users  $k_r$  at reflect area and  $k_t$  at transmit area can be expressed as:

$$y_{k_r} = \sqrt{\frac{\rho \zeta P_s}{d_{BV}^\alpha d_{VU_r}^\alpha}} \left[ \sum_{i=1}^M h_i e^{-j\vartheta_r^m} g_{r_i} \right] x_r + n_r, \quad (2)$$

$$y_{k_t} = \sqrt{\frac{(1-\rho)(1-\zeta)P_s}{d_{BV}^\alpha d_{VU_t}^\alpha}} \left[ \sum_{i=1}^M h_i e^{-j\vartheta_t^m} g_{t_i} \right] x_t + \sqrt{\frac{\rho \zeta P_s}{d_{BV}^\alpha d_{VE}^\alpha}} \left[ \sum_{i=1}^M h_i e^{-j\vartheta_t^m} g_{t_i} \right] x_r + n_t. \quad (3)$$

Similarly, the received signals at each Eavesdropper in both areas are given by:

$$y_{e_r} = \sqrt{\frac{\rho \zeta P_s}{d_{BV}^\alpha d_{VE}^\alpha}} \left[ \sum_{i=1}^M h_i e^{-j\vartheta_r^m} g_{e_{r_i}} \right] x_r + n_{e_r}, \quad (4)$$

$$y_{e_t} = \sqrt{\frac{(1-\rho)(1-\zeta)P_s}{d_{BV}^\alpha d_{VE}^\alpha}} \left[ \sum_{i=1}^M h_i e^{-j\vartheta_t^m} g_{e_{t_i}} \right] x_t$$

$$+ \sqrt{\frac{\rho \zeta P_s}{d_{BV}^\alpha d_{VE}^\alpha}} \left[ \sum_{i=1}^M h_i e^{-j\vartheta_t^m} g_{e_{t_i}} \right] x_r + n_{e_t}. \quad (5)$$

where  $d_{BV} = \sqrt{(x_b - x_u)^2 + (y_b - y_u)^2 + (z_b - z_u)^2}$  denotes the Euclidean distances between the BS and UAV,  $d_{VU_q} = \sqrt{(x_{k_q} - x_u)^2 + (y_{k_q} - y_u)^2 + z_u^2}$  denotes the Euclidean distances between the STAR-RIS and LU  $k$ , and  $d_{VE_q} = \sqrt{(x_{e_q} - x_u)^2 + (y_{e_q} - y_u)^2 + z_u^2}$  denotes the Euclidean distances between the STAR-RIS and Eve.  $\epsilon$  is the corresponding path loss exponents. The phase shifts  $\vartheta_r^m$  and  $\vartheta_t^m$  can be independently adjusted.  $n \sim \mathcal{CN}(0, N_0)$  represents the additive white Gaussian noise (AWGN) and  $N_0$  is the variance. However, imperfections from jittering and airflow make precise adjustment of the reflecting elements challenging, resulting in practical phase shifts with error  $\phi$ , thus:

$$\theta_q^m = \theta_{opt} + \phi. \quad (6)$$

Under the NOMA framework, LUs perform successive interference cancellation (SIC) according to a decoding order. Without loss of generality, this order is assumed to correspond to descending channel gains across the  $K$  LUs. Then, the signal-interference-to-noise ratio (SINR) at the LUs  $\{k_r, k_t\}$  using (2) and (3), can be given by:

$$\gamma_{k_r} = \frac{\rho \zeta P_s \left| \sum_{i=1}^M h_i g_{r_i} e^{-j\vartheta_r^m} \right|^2}{N_0 d_{BV}^\alpha d_{VU_r}^\alpha}, \quad (7)$$

$$\gamma_{k_t} = \frac{(1-\rho) \frac{(1-\zeta)P_s}{d_{BV}^\alpha d_{VU_t}^\alpha} \left| \sum_{i=1}^M h_i g_{t_i} e^{-j\vartheta_t^m} \right|^2}{\rho \frac{\zeta P_s}{d_{BV}^\alpha d_{VE}^\alpha} \left| \sum_{i=1}^M h_i g_{t_i} e^{-j\vartheta_t^m} \right|^2 + N_0}, \quad (8)$$

and, the data rate of LU is  $R_{k_q} = \log_2(1 + \gamma_{k_q})$ . Moreover, the SINR at the eavesdroppers  $\{e_r, e_t\}$  for decoding the signal of BS using (4) and (5), can be given by:

$$\gamma_{e_r} = \frac{\rho \zeta P_s \left| \sum_{i=1}^M h_i g_{e_{r_i}} e^{-j\vartheta_r^m} \right|^2}{N_0 d_{BV}^\alpha d_{VE_r}^\alpha}, \quad (9)$$

$$\gamma_{e_t} = \frac{(1-\rho) \frac{(1-\zeta)P_s}{d_{BV}^\alpha d_{VE_t}^\alpha} \left| \sum_{i=1}^M h_i g_{e_{t_i}} e^{-j\vartheta_t^m} \right|^2}{\rho \frac{\zeta P_s}{d_{BV}^\alpha d_{VE}^\alpha} \left| \sum_{i=1}^M h_i g_{e_{t_i}} e^{-j\vartheta_t^m} \right|^2 + N_0}. \quad (10)$$

Similarly, we can obtain the data rate of eavesdroppers for decoding the signal of BS as  $R_{e_q} = \log_2(1 + \gamma_{e_q})$ . Accordingly, the secrecy rate is defined as the difference between the achievable data rate of each user and that of the eavesdroppers in both the reflection and transmission regions, which is given by:

$$R_{rn}^{sec} = [R_{k_r} - R_{r_{ne}}]^+, \quad (11)$$

$$R_{tn}^{sec} = [R_{k_t} - R_{t_{ne}}]^+. \quad (12)$$

Therefore, the sum secure rate of a pair is

$$R^{sec} = R_{rn}^{sec} + R_{tn}^{sec}, \quad (13)$$

where  $[u]^+ = \max\{u, 0\}$ .

## B. SNR Distribution

The signal-to-noise ratio (SNR) at the user LU is influenced by the phase shifts of the reflecting elements of the RIS. The optimal phase shift  $\theta_{op}$  for the  $n$ -th reflecting element is given by:

$$\theta_{opt} = -(\theta_{h_i} + \theta_{g_{q_i}}), \quad (14)$$

where  $\theta_{h_i}$  and  $\theta_{g_{q_i}}$  are the phases of the channels  $h_i$  and  $g_{q_i}$ , respectively.

1) *Phase Estimation Errors*: Due to practical imperfections such as jittering and airflow effects, the actual phase shift  $\theta_q^m$  deviates from the optimal phase:

$$\theta_q^m = \theta_{opt} + \phi. \quad (15)$$

The phase estimation error  $\phi$  follows a von-Mises distribution with zero mean and concentration parameter  $k$ . The probability density function (PDF) and eigen function of  $\phi$ , respectively, are given by

$$f_\phi(x) = \frac{e^{k \cos(x)}}{2\pi I_0(k)}, \quad (16)$$

$$\varphi_p = \mathbb{E}(e^{ip\phi}) = \frac{I_p(k)}{I_0(k)}. \quad (17)$$

where  $I_0(\cdot)$  and  $I_p(\cdot)$  are the modified Bessel functions of the first kind of order zero and  $p$ , respectively.

2) *SNR Expressions*: Under phase estimation errors, the SNRs of users  $\{k_r, k_t\}$  can be expressed as:

$$\gamma_{k_r} = \frac{\rho\zeta P_s \left| \sum_{i=1}^M h_i g_{r_i} e^{-j\theta_{r_i}} \right|^2}{N_0 d_{BV}^\alpha d_{VUr}^\alpha} = k_1 X_r, \quad (18)$$

$$\begin{aligned} \gamma_{k_t} &= \frac{(1-\rho) \frac{(1-\zeta)P_s}{d_{BV}^\alpha d_{VUt}^\alpha} \left| \sum_{i=1}^M h_i g_{t_i} e^{-j\theta_{t_i}} \right|^2}{\rho \frac{\zeta P_s}{d_{BV}^\alpha d_{VUr}^\alpha} \left| \sum_{i=1}^M h_i g_{t_i} e^{-j\theta_{t_i}} \right|^2 + N_0} \\ &= \frac{k_2 X_t}{k_1 X_t + 1}, \end{aligned} \quad (19)$$

where  $k_1 = \frac{\rho\zeta P_s}{N_0 d_{BV}^\alpha d_{VUr}^\alpha}$  and  $k_2 = \frac{(1-\rho)(1-\zeta)P_s}{N_0 d_{BV}^\alpha d_{VUt}^\alpha}$ , with  $P_s$  denoting the transmitting power BS, as previously stated, we employ Nakagami- $m$  fading model to characterize the small-scale fading of A2G channels, due to its ability to represent a wide variety of multipath fading conditions by adjusting the fading severity parameter  $m$ , where by denoting  $X_q = \left| \sum_{i=1}^M |h_i| |g_{q_i}| e^{-j\phi_i} \right|^2 = |U_q + jV_q|^2$  the expectations and variances of  $U_q$  can be obtained as:

$$\mathbb{E}(U_r) = M\mathbb{E}(|h_i| |g_{r_i}| \cos \phi_i) = M\alpha_r^2 \Phi,$$

$$\begin{aligned} V(U_r) &= M\mathbb{E}(|h_i| |g_{r_i}| \cos \phi_i)^2 - M\mathbb{E}^2(|h_i| |g_{r_i}| \cos \phi_i) \\ &= \frac{M}{2}(1 + \varphi_2 - 2\alpha_r^4 \varphi_1^2), \end{aligned}$$

where  $\alpha_q = \sqrt{\mathbb{E}(|h_i| \mathbb{E}(|g_{q_i}|))}$ ,  $\mathbb{E}(|h_i|) = \frac{\Gamma(m_{BV}+0.5)}{\Gamma(m_{BV})\sqrt{m_{BV}}}$  and  $\mathbb{E}(|g_{q_i}|) = \frac{\Gamma(m_{VUq}+0.5)}{\Gamma(m_{VUq})\sqrt{m_{VUq}}}$ .

*Proof*: Please refer to Appendix A and B.

According to [42], the PDF of  $X_q$  is given by:

$$f_{X_q}(x) = \frac{x^{m_{BVUq}-1} m_{BVUq}^{m_{BVUq}} e^{-\frac{m_{BVUq}x}{\Omega_{BVUq}}}}{\Gamma(m_{BVUq}) \Omega_{BVUq}^{m_{BVUq}}} e^{-\frac{m_{BVUq}x}{\Omega_{BVUq}}}. \quad (20)$$

where  $m_{BVU} = \frac{\mathbb{E}^2(U_q)}{4V(U_q)} = \frac{M\alpha_q^4 \varphi_1^2}{2(1+\varphi_2-2\alpha_q^4 \varphi_1^2)}$ ,  $\Omega_{BVU_r} = \mathbb{E}^2(U_q) = M^2 \alpha_q^4 \varphi_1^2$ .

For the eavesdropper, the phase shifts are optimized with respect to the legitimate user's channel, leading to a different effective phase shift expression at the eavesdropper, which may cause signal misalignment and reduce the received signal strength. It will no longer depend on a single  $\phi$ , but it will include three key angular components  $\theta_{eff} = \theta_{g_{eq}} - \theta_{g_q} + \phi$  where,  $\phi \sim$  von Mises distribution with zero mean and concentration parameter  $k$ ,  $\{\theta_{g_{eq}}, \theta_{g_q}\}$  are uniformly distributed over  $[0, 2\pi)$ , representing the unknown phases of the eavesdropper and legitimate user channels, respectively.

The composite error  $\theta_{eff}$  can be approximated as a wrapped normal random variable with zero mean and variance  $Var(\theta_{eff}) = Var(\theta_{g_{eq}}) - Var(\theta_{g_q}) + Var(\phi)$ . Considering Nakagami,  $X_{e_q} = \left| \sum_{i=1}^M |h_i| |g_{e_{q_i}}| e^{-j(\theta_{g_{e_{q_i}}} - \theta_{g_{r_i}} + \phi_i)} \right|^2 = |U_{e_q} + jV_{e_q}|^2$ .

Therefore, the instantaneous SNRs for eavesdroppers in the reflect and transmit areas are derived as follows:

$$\gamma_{r_{ne}} = \frac{\rho\zeta P_s \left| \sum_{i=1}^M h_i g_{e_{r_i}} e^{-j(\theta_{opt_i} + \theta_{eff_i})} \right|^2}{N_0 d_{BV}^\alpha d_{VEr}^\alpha} = k'_1 X_{er}, \quad (21)$$

where  $k'_1 = \frac{\rho\zeta P_s}{N_0 d_{BV}^\alpha d_{VEr}^\alpha}$ , and  $X_{er} = \left| \sum_{i=1}^M |h_i| |g_{e_{r_i}}| e^{-j\theta_{eff_i}} \right|^2$ .

$$\begin{aligned} \gamma_{t_{ne}} &= \frac{\frac{(1-\rho)(1-\zeta)P_s}{d_{BV}^\alpha d_{VEt}^\alpha} \left| \sum_{i=1}^M h_i g_{e_{t_i}} e^{-j(\theta_{opt_i} + \theta_{eff_i})} \right|^2}{\rho \frac{\zeta P_s}{d_{BV}^\alpha d_{VEr}^\alpha} \left| \sum_{i=1}^M h_i g_{e_{t_i}} e^{-j(\theta_{opt_i} + \theta_{eff_i})} \right|^2 + N_0} \\ &= \frac{k'_2 X_{et}}{k'_1 X_{et} + 1}, \end{aligned} \quad (22)$$

where  $k'_1 = \frac{\rho\zeta P_s}{N_0 d_{BV}^\alpha d_{VEr}^\alpha}$ ,  $k'_2 = \frac{(1-\rho)(1-\zeta)P_s}{N_0 d_{BV}^\alpha d_{VEt}^\alpha}$ . The expectations and variances of  $U_{e_q}$  can be obtained as:

$$\mathbb{E}(U_{er}) = M\mathbb{E}(|h_i| |g_{e_{r_i}}| \cos(\theta_{eff_i})) = M\alpha_{e_q}^2 \Phi,$$

$$\begin{aligned} V(U_{e_q}) &= M\mathbb{E}(|h_i| |g_{e_{q_i}}| \cos \theta_{eff_i})^2 - M\mathbb{E}^2(|h_i| |g_{e_{q_i}}| \cos \theta_{eff_i}) \\ &= \frac{M}{2}(1 + \varphi_2 - 2\alpha_{e_q}^4 \Phi^2), \end{aligned}$$

where  $\Phi = e^{-\frac{Var(\theta_{eff_i})}{2}}$ ,  $\alpha_{e_q} = \sqrt{\mathbb{E}(|h_i| \mathbb{E}(|g_{e_{q_i}}|))}$ , and  $\mathbb{E}(|g_{e_{q_i}}|) = \frac{\Gamma(m_{VEq}+0.5)}{\Gamma(m_{VEq})\sqrt{m_{VEq}}}$ .

Therefore, the PDF of  $X_{er}$  is given by:

$$f_{X_{e_q}}(x) = \frac{x^{m_{BVEq}-1} m_{BVEq}^{m_{BVEq}} e^{-\frac{m_{BVEq}x}{\Omega_{BVEq}}}}{\Gamma(m_{BVEq}) \Omega_{BVEq}^{m_{BVEq}}} e^{-\frac{m_{BVEq}x}{\Omega_{BVEq}}}, \quad (23)$$

where  $m_{BVEq} = \frac{M\alpha_{e_q}^4 \Phi^2}{2(1+\varphi_2-2\alpha_{e_q}^4 \Phi^2)}$ , and  $\Omega_{BVEq} = \frac{M^2 \alpha_{e_q}^4 \Phi^2}{m_{BVEq}}$ .

### III. PERFORMANCE ANALYSIS

This section derives a precise expression for the ergodic secrecy rate applicable to both reflection and transmission regions in the STAR-RIS-assisted NOMA system, taking into account different UAV positions and power allocation schemes.

#### A. Ergodic Secrecy Rate of the Transmit Area

The ergodic capacity of the users  $k_t$  at the transmit area is expressed as:

$$\begin{aligned} C_{k_t} &= \frac{1}{\ln(2)} \mathbb{E}[\log_2(1 + \gamma_{k_t})] \\ &= \frac{1}{\ln(2)} \mathbb{E}[\log_2(1 + (\frac{k_2 X_t}{k_1 X_t + 1}))]. \end{aligned} \quad (24)$$

Based on [43], a moment generating function (MGF)-based expression for the ergodic capacity is presented as:

$$\begin{aligned} &\mathbb{E}[\ln(\frac{k_2 X_t}{k_1 X_t + 1})] \\ &= \int_0^\infty \frac{\mathcal{M}_{X_t}(k_1 z) - \mathcal{M}_{X_t}((k_1 + k_2)z)}{z} e^{-z} dz. \end{aligned}$$

It is noteworthy that  $\mathcal{M}_X(\beta z) = \mathbb{E}[e^{-z\beta X}]$  is the MGF of  $\beta X$ ,  $\beta \in \{k_1, (k_1 + k_2)\}$ . Therefore,

$$\begin{aligned} \mathcal{M}_{X_t}(k_1 z) &= E[e^{-zk_1 X}] = \int_0^\infty e^{-zk_1 X} f_{X_t}(x) dx \\ &= \int_0^\infty e^{-zk_1 X} \cdot \frac{x^{m_{BVU_t}-1} m_{BVU_t}^{m_{BVU_t}}}{\Gamma(m_{BVU_t}) \Omega_{BVU_t}^{m_{BVU_t}}} e^{-\frac{m_{BVU_t}}{\Omega_{BVU_t}} x} dx \\ &= \left(1 + \frac{z \Omega_{BVU_t} k_1}{m_{BVU_t}}\right)^{-m_{BVU_t}}, \end{aligned} \quad (25)$$

and

$$\begin{aligned} \mathcal{M}_{X_t}((k_2 + k_1)z) &= \int_0^\infty e^{-z(k_1+k_2)X} f_{X_t}(x) dx \\ &= \int_0^\infty e^{-z(k_1+k_2)X} \cdot \frac{x^{m_{BVU_t}-1} m_{BVU_t}^{m_{BVU_t}}}{\Gamma(m_{BVU_t}) \Omega_{BVU_t}^{m_{BVU_t}}} e^{-\frac{m_{BVU_t}}{\Omega_{BVU_t}} x} dx \\ &= \left(1 + \frac{z \Omega_{BVU_t} (k_2 + k_1)}{m_{BVU_t}}\right)^{-m_{BVU_t}}. \end{aligned} \quad (26)$$

Therefore,

$$\begin{aligned} C_{k_t} &= \frac{1}{\ln(2)} \int_0^\infty \frac{e^{-z}}{z} \left[ \left(1 + \frac{z \Omega_{BVU_t} k_1}{m_{BVU_t}}\right)^{-m_{BVU_t}} \right. \\ &\quad \left. - \left(1 + \frac{z \Omega_{BVU_t} (k_2 + k_1)}{m_{BVU_t}}\right)^{-m_{BVU_t}} \right] dz. \end{aligned} \quad (27)$$

Furthermore, the expression given in (27) can be written in terms of the weights and sample points of the Laguerre orthogonal polynomial as

$$C_{k_t} = \frac{1}{\ln(2)} \sum_{i=1}^N \frac{w_i}{z_i} \left[ \left(1 + \frac{\Omega_{BVU_t} \rho \zeta P_s z_i}{N_0 m_{BVU_t} d_{BV}^\alpha d_{VU_t}^\alpha}\right)^{-m_{BVU_t}} \right.$$

$$\left. - \left[1 + \frac{\Omega_{BVU_t} z_i (1 - \rho - \zeta + 2\rho\zeta) P_s}{m_{BVU_t} N_0 d_{BV}^\alpha d_{VU_t}^\alpha}\right]^{-m_{BVU_t}} \right]. \quad (28)$$

Similarly, we can obtain the ergodic capacity of the eavesdropper at the transmit area as follows

$$C_{e_t} = \frac{1}{\ln(2)} \int_0^\infty \frac{\mathcal{M}_{X_t}(k'_1 z) - \mathcal{M}_{X_t}((k'_1 + k'_2)z)}{z} e^{-z} dz,$$

where

$$\begin{aligned} \mathcal{M}_{X_e}(k'_1 z) &= \mathbb{E}[e^{-zk'_1 X_e}] \\ &= \int_0^\infty e^{-zk'_1 X_e} f_{X_e}(x) dx \\ &= \int_0^\infty e^{-zk'_1 X_e} \frac{x^{m_{BVE_t}-1} m_{BVE_t}^{m_{BVE_t}}}{\Gamma(m_{BVE_t}) \Omega_{BVE_t}^{m_{BVE_t}}} e^{-\frac{m_{BVE_t}}{\Omega_{BVE_t}} x} dx \\ &= \left(1 + \frac{z \Omega_{BVE_t} k'_1}{m_{BVE_t}}\right)^{-m_{BVE_t}}, \end{aligned} \quad (29)$$

and

$$\begin{aligned} \mathcal{M}_{X_t}((k'_2 + k'_1)z) &= \int_0^\infty e^{-z(k'_1+k'_2)X_e} f_{X_e}(x) dx \\ &= \int_0^\infty e^{-z(k_1+k_2)X_e} \frac{x^{m_{BVE_t}-1} m_{BVE_t}^{m_{BVE_t}}}{\Gamma(m_{BVE_t}) \Omega_{BVE_t}^{m_{BVE_t}}} e^{-\frac{m_{BVE_t}}{\Omega_{BVE_t}} x} dx \\ &= \left(1 + \frac{z \Omega_{BVE_t} (k'_1 + k'_2)}{m_{BVE_t}}\right)^{-m_{BVE_t}}. \end{aligned} \quad (30)$$

Therefore,

$$\begin{aligned} C_{e_t} &= \frac{1}{\ln(2)} \int_0^\infty \frac{1}{z} e^{-z} \left[ \left(1 + \frac{z \Omega_{BVE_t} k'_1}{m_{BVE_t}}\right)^{-m_{BVE_t}} \right. \\ &\quad \left. - \left(1 + \frac{z \Omega_{BVE_t} (k'_1 + k'_2)}{m_{BVE_t}}\right)^{-m_{BVE_t}} \right] dz. \end{aligned} \quad (31)$$

The expression given in (27), can be written in terms of the weights and sample points of the Laguerre orthogonal polynomial as

$$\begin{aligned} C_{e_t} &= \frac{1}{\ln(2)} \sum_{i=1}^N \frac{w_i}{z_i} \left( \left(1 + \frac{\Omega_{BVE_t} \rho \zeta P_s z_i}{N_0 m_{BVE_t} d_{BV}^\alpha d_{VE_t}^\alpha}\right)^{-m_{BVE_t}} \right. \\ &\quad \left. - \left(1 + \frac{\Omega_{BVE_t} z_i (1 - \rho - \zeta + 2\rho\zeta) P_s}{m_{BVE_t} N_0 d_{BV}^\alpha d_{VE_t}^\alpha}\right)^{-m_{BVE_t}} \right). \end{aligned} \quad (32)$$

Based on (12) the secrecy rate can be obtain as:

$$\begin{aligned} R_t^{sec} &= \left[ \frac{1}{\ln(2)} \sum_{i=1}^N \frac{w_i}{z_i} \left( \left(1 + \frac{\Omega_{BVU_t} \rho \zeta P_s z_i}{N_0 m_{BVU_t} d_{BV}^\alpha d_{VU_t}^\alpha}\right)^{-m_{BVU_t}} \right. \right. \\ &\quad \left. \left. - \left(1 + \frac{\Omega_{BVU_t} z_i (1 - \rho - \zeta + 2\rho\zeta) P_s}{m_{BVU_t} N_0 d_{BV}^\alpha d_{VU_t}^\alpha}\right)^{-m_{BVU_t}} \right) \right] \end{aligned}$$

$$\begin{aligned}
& - \left( 1 + \frac{\Omega_{BVE_t} \rho \zeta P_s z_i}{N_0 m_{BVE_t} d_{BV}^\alpha d_{VE_t}^\alpha} \right)^{-m_{BVE_t}} \\
& + \left( 1 + \frac{\Omega_{BVE_t} z_i (1 - \rho - \zeta + 2\rho\zeta) P_s}{m_{BVE_t} N_0 d_{BV}^\alpha d_{VE_t}^\alpha} \right)^+ \Big]. \quad (33)
\end{aligned}$$

### B. Ergodic Secrecy Rate of the Reflect Area

The ergodic capacity of the user  $k_r$  at the reflect area is expressed as:

$$\begin{aligned}
C_{k_r} &= \frac{1}{\ln(2)} \mathbb{E} [\log_2(1 + \gamma_{k_r})] = \frac{1}{\ln(2)} \mathbb{E} [\ln(1 + k_1 X_r)] \\
&= \frac{1}{\ln(2)} \mathbb{E} \left[ \log_2 \left( 1 + \frac{\rho \zeta P_s \left| \sum_{i=1}^M h_i g_{r_i} e^{-j\phi_i} \right|^2}{N_0 d_{BV}^\alpha d_{VU_r}^\alpha} \right) \right] \\
&= \frac{1}{\ln(2)} \int_0^\infty \frac{1 - \mathcal{M}_{X_r}(z)}{z} e^{-z} dz \\
&= \frac{1}{\ln(2)} \int_0^\infty \frac{1 - \left( 1 + \frac{z \Omega_{BVU_r} k_1}{m_{BVU_r}} \right)^{-m_{BVU_r}}}{z} e^{-z} dz, \quad (34)
\end{aligned}$$

where  $\mathcal{M}_{X_r}(k_1 z) = \left( 1 + \frac{z \Omega_{BVU_r} k_1}{m_{BVU_r}} \right)^{-m_{BVU_r}}$ , the expression given in (30), can be written as

$$\begin{aligned}
C_{k_r} &= \frac{1}{\ln(2)} \sum_{i=1}^N \frac{w_i}{z_i} \\
& \left[ 1 - \left( 1 + \frac{\Omega_{BVU_r} \rho \zeta P_s z_i}{N_0 m_{BVU_r} d_{BV}^\alpha d_{VU_r}^\alpha} \right)^{-m_{BVU_r}} \right]. \quad (35)
\end{aligned}$$

Similarly, we can obtain the ergodic capacity of the eavesdropper as follows

$$\begin{aligned}
C_{e_r} &= \frac{1}{\ln(2)} \mathbb{E} [\log_2(1 + \gamma_{e_r})] = \frac{1}{\ln(2)} \mathbb{E} [\ln(1 + k'_1 X_{e_r})] \\
&= \frac{1}{\ln(2)} \int_0^\infty \frac{1 - \mathcal{M}_{X_{e_r}}(z)}{z} e^{-z} dz \\
&= \frac{1}{\ln(2)} \int_0^\infty \frac{1 - \left( 1 + \frac{z \Omega_{BVE_r} k'_1}{m_{BVE_r}} \right)^{-m_{BVE_r}}}{z} e^{-z} dz. \quad (36)
\end{aligned}$$

Therefore, the expression given in (36) can be written as:

$$\begin{aligned}
C_{e_r} &= \frac{1}{\ln(2)} \sum_{i=1}^N \frac{w_i}{z_i} \\
& \left[ 1 - \left( 1 + \frac{\Omega_{BVE_r} \rho \zeta P_s z_i}{N_0 m_{BVE_r} d_{BV}^\alpha d_{VE_r}^\alpha} \right)^{-m_{BVE_r}} \right]. \quad (37)
\end{aligned}$$

Based on (11) the secrecy rate can be obtained as:

$$\begin{aligned}
R_r^{sec} &= \left[ \frac{1}{\ln(2)} \sum_{i=1}^N \frac{w_i}{z_i} \left( \left( 1 + \frac{\Omega_{BVE_r} \rho \zeta P_s z_i}{N_0 m_{BVE_r} d_{BV}^\alpha d_{VE_r}^\alpha} \right)^{-m_{BVE_r}} \right. \right. \\
& \left. \left. - \left( 1 + \frac{\Omega_{BVU_r} \rho \zeta P_s z_i}{N_0 m_{BVU_r} d_{BV}^\alpha d_{VU_r}^\alpha} \right)^{-m_{BVU_r}} \right) \right]^+. \quad (38)
\end{aligned}$$

## IV. JOINT OPTIMIZATION OF WSSR

In this section, we adopt an alternating optimization (AO) approach to solve the non-convex joint optimization problem in (39), which involves two key variables: the UAV's 3D placement and the power allocation ratio of the STAR-RIS. Specifically, the original problem is decomposed into two subproblems, each solved iteratively while fixing the other variable. For the UAV placement subproblem, which is non-convex due to the complex dependence of the secrecy rate on the UAV's position, we employ the 3D search algorithm method to obtain an efficient solution. For the second subproblem involving the non-convex STAR-RIS power allocation ratio, we apply a one-dimensional search or approximation-based method to determine the optimal power split between the transmission and reflection regions.

$$\max_{C_u, \zeta} w_1 R_t^{sec} + w_2 R_r^{sec} \quad (39a)$$

$$s.t. \quad w_1 + w_2 = 1, w_1, w_2 \in [0, 1], w_1 < w_2 \quad (39b)$$

$$x_{min} \leq x_u \leq x_{max} \quad (39c)$$

$$y_{min} \leq y_u \leq y_{max} \quad (39d)$$

$$z_{min} \leq z_u \leq z_{max} \quad (39e)$$

$$\zeta_t^m + \zeta_r^m = 1, \zeta_q^m \in [0, 1], q \in [r, t], \forall m. \quad (39f)$$

### A. Optimization of UAV Placement

In this subsection, we optimize the UAV's 3D positioning through linear grid-based search algorithm where two coordinates are held fixed while the third is adjusted iteratively. This strategy ensures systematic convergence toward an optimal location that maximizes the secrecy rate. Therefore, given the power allocation  $\zeta$  the optimization problem of UAV position can be separated from (39) as:

$$\max_{C_u} w_1 R_t^{sec} + w_2 R_r^{sec} \quad (40a)$$

$$s.t. \quad w_1 + w_2 = 1, w_1, w_2 \in [0, 1], w_1 < w_2 \quad (40b)$$

$$x_{min} \leq x_u \leq x_{max} \quad (40c)$$

$$y_{min} \leq y_u \leq y_{max} \quad (40d)$$

$$z_{min} \leq z_u \leq z_{max}. \quad (40e)$$

In this subsection, we focus on optimizing the 3D placement of the UAV to maximize the WSSR under a given power allocation configuration  $\zeta$  of the STAR-RIS. However, the problem is inherently non-convex, as the secrecy rate expressions are complex and non-linear functions of the UAV's coordinates. To efficiently tackle this challenge, we adopt a grid-based iterative coordinate descent approach, where at each step, two coordinates are held fixed while the third is optimized over a discretized search space. This process is cyclically repeated over the three dimensions until it is reached. Such a strategy enables systematic exploration of the 3D position space and provides a practical solution with reasonable computational complexity. The iterative algorithm to solve this subproblem is detailed in Algorithm 1.

**Algorithm 1** Iterative algorithm for problem (40)

1. Initial UAV position  $x_u, y_u, z_u$ , where  $x = x_{\min} : 1 : x_{\max}$ ,  $y = y_{\min} : 1 : y_{\max}$ ,  $z = z_{\min} : 1 : z_{\max}$ . Set iteration index  $k = 1$ , and convergence threshold  $\epsilon_0 > 0$ .
2. Fix  $x_u^{(k)}, y_u^{(k)}$ , search over  $z_u \in [z_{\min}, z_{\max}]$ .
3. Evaluate the objective  $w_1 R_t^{sec} + w_2 R_r^{sec}$ .
4. Select  $z_u^{(k+1)}$  that maximizes the WSSR.
5. Fix  $z_u^{(k+1)}, y_u^{(k)}$ , search over  $x_u \in [x_{\min}, x_{\max}]$ .
6. Repeat the evaluation and update  $x_u^{(k+1)}$ .
7. Fix  $z_u^{(k+1)}, x_u^{(k+1)}$ , search over  $y_u \in [y_{\min}, y_{\max}]$ .
8. Repeat the evaluation and update  $y_u^{(k+1)}$ .
9. Check convergence:  $\|C_u^{(k+1)} - C_u^{(k)}\| < \epsilon_0$ .
10. Break.
11. Set  $k \leftarrow k + 1$  Until  $\{k = K_{\max}\}$ .
12. Return.
13.  $(x_u^*, y_u^*, z_u^*) = C_u^{(k+1)}$ .

**B. Optimization of Power Allocation**

Given the optimized UAV position  $C_u$ , we aim to further enhance the secrecy performance of the system while ensuring fairness between users. To this end, we adopt a power allocation strategy that maximizes the WSSR. The corresponding optimization problem is defined as follows:

$$\max_{\zeta} w_1 R_t^{sec} + w_2 R_r^{sec} \quad (41a)$$

$$s.t. \quad w_1 + w_2 = 1, w_1, w_2 \in [0, 1], w_1 < w_2 \quad (41b)$$

$$\zeta_t^m + \zeta_r^m = 1, \zeta_q^m \in [0, 1], q \in [r, t], \forall m. \quad (41c)$$

To address the non-convexity of the WSSR function with respect to  $\zeta$ , we employ the Golden Section Search (GSS) algorithm. This method is highly suitable for solving one-dimensional unimodal optimization problems, offering a balance between accuracy and computational efficiency. The GSS technique iteratively narrows the search interval for  $\zeta$ , converging to the optimal value that maximizes the WSSR under the given fairness and feasibility constraints. The iterative algorithm to solve this subproblem is detailed in Algorithm 2.

**V. NUMERICAL RESULTS**

In this section, we investigate a wireless communication system comprising three legitimate users and three eavesdroppers operating in both reflect and transmit areas. The BS is positioned at coordinates (5, 5, 5), while legitimate users in the reflect area are located at (1, 1, 0), (0.5, 0.5, 0), (2, 0.5, 0), and those in the transmit area at (-1, -1, 0), (-0.5, -0.5, 0), (-2, -0.5, 0). Eavesdroppers are placed at (2, 2, 0), (0.25, 0.25, 0), (2, 1.5, 0), in the reflect area and (-2, -2, 0), (-0.25, -0.25, 0), (-2, -1.5, 0) in the transmit area, and the UAV is positioned at coordinates (0.5, 0.5, 10). The system employs Nakagami- $m$  fading channels with a severity parameter of  $m = 2$  for all links. In the reflect region, the STAR-RIS power coefficient  $\zeta$  is set to 0.2, indicating 20% power allocated for reflection, while the NOMA power-splitting coefficient  $\rho$  is set to 0.3, allocating 30% of the transmit power to users in the reflect

**Algorithm 2** GSS for Optimal Power Allocation

1. Initial search interval  $[a, b] = [0, 1]$ , tolerance  $\epsilon > 0$ , weights  $w_1, w_2$  satisfying  $w_1 + w_2 = 1$  and  $w_1 < w_2$ , golden ratio  $\varphi = (\sqrt{5} - 1)/2 \approx 0.618$ , Set iteration index  $n = 0$ .
2. Compute initial points  $c = b - \varphi(b - a), d = a + \varphi(b - a)$ .
3. Evaluate WSSR at  $c$  and  $d$  :  
 $f_c = w_1 R_t^{sec}(c) + w_2 R_r^{sec}(c), f_d = w_1 R_t^{sec}(d) + w_2 R_r^{sec}(d)$ .
4. While  $(b - a > \epsilon)$  and  $(n < N_{\max})$ :
5. If  $f_c > f_d$ :
6. Set  $b = d, d = c$ , and  $c = b - \varphi(b - a)$ ,
7. Update  $f_d = f_c$ .
8. Compute  $f_c = w_1 R_t^{sec}(c) + w_2 R_r^{sec}(c)$
9. Else:
10. Set  $a = c, c = d$  and  $d = a + \varphi(b - a)$ .
11. Update  $f_c = f_d$ .
12. Compute  $f_d = w_1 R_t^{sec}(d) + w_2 R_r^{sec}(d)$ .
13. Set  $n \leftarrow n + 1$ .
14. Return optimal  $\zeta^* = (a + b)/2$ .

area. To verify our analysis, Monte Carlo simulation results are provided. Secrecy performance is evaluated across transmit power levels ranging from 0 to 50 dBm. This analysis offers key insights into the power-security trade-offs for dual-area systems with spatially distributed adversaries, highlighting the critical role of directional interference management in enhancing PLS.

Fig. 2 shows the secrecy rate versus transmit power in the transmit area of a STAR-RIS-assisted UAV NOMA system under different values of the concentration parameter  $k$  of the von Mises distribution. The plot includes both analytical and Monte Carlo (MC) simulation results for  $k = 10, 15, 20$ , where a higher  $k$  value indicates lower phase uncertainty and more accurate phase alignment. As the transmit power increases, the secrecy rate initially improves due to enhanced signal quality at the legitimate user compared to the eavesdropper. However, beyond a certain power level (around 25–50 dBm), the secrecy rate begins to decline. This is because high transmit power also benefits the eavesdropper and amplifies the negative effects of residual phase errors and inter-user interference in the NOMA system. Moreover, lower  $k$  values (e.g.,  $k = 10$ ) correspond to higher phase uncertainty, which reduces beamforming accuracy and degrades secrecy performance. In contrast, higher  $k$  values (e.g.,  $k = 20$ ) lead to more focused phase distributions, resulting in improved secrecy rates.

Unlike in the transmit area, the secrecy rate in Fig. 3 monotonically increases with transmit power and does not peak or decline. This trend indicates that, in the reflect area, the benefit of increased transmit power consistently outweighs the negative effects of inter-user interference and phase estimation errors. As the transmit power increases, the SNR at the legitimate user improves significantly, leading to a higher achievable rate. The eavesdropper, however, experiences only limited gain from increased power due to the suboptimal STAR-RIS alignment and less favorable propagation conditions in the reflect region. This asymmetric improvement leads to a steadily growing secrecy rate. Moreover, as the von Mises concentration parameter  $k$  increases implying lower

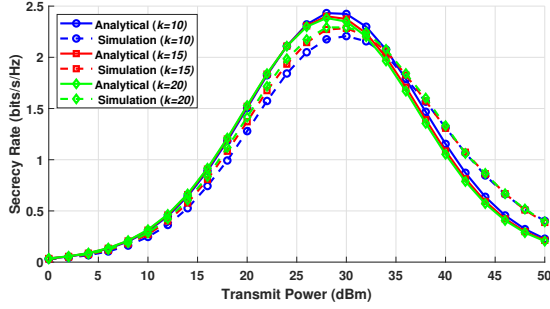


Figure 2. The secrecy rate versus the transmit power for the transmit area with different values of  $\kappa$ .

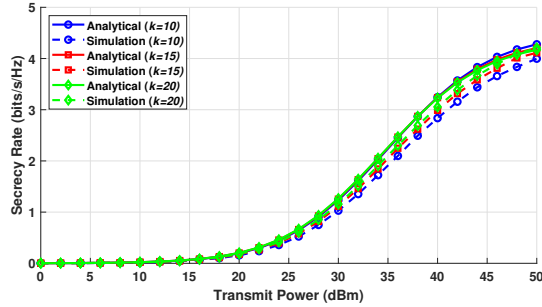


Figure 3. The secrecy rate versus the transmit power for the reflect area with different values of  $\kappa$ .

phase noise and more accurate RIS phase control the system achieves better beamforming precision. Consequently, the secrecy rate improves with higher  $k$ . The reflect area exhibits a more gradual improvement in its secrecy rate  $R_r^{sec}$ . Although there is an upward trend, the rate of increase is noticeably slower compared to the transmit area. This difference can be attributed to the inherent characteristics of the reflect area, where additional challenges such as multipath propagation and reduced direct signal strength can impede performance. The eavesdropper's capacity in this environment improves at a different rate than that of the legitimate user, leading to a less pronounced enhancement in secrecy rates. Adjusting the value  $\rho = 0.3$  directly influences the power allocation between the reflect and transmit areas. Specifically,  $\rho$  determines the fraction of power allocated to the reflect area, while  $(1 - \rho)$  is allocated to the transmit area. A lower value of  $\rho$  (that is, allocating less power to the reflect area and more to the transmit area) enhances the performance in the transmit region, thereby increasing the secrecy rate due to better signal quality for legitimate users and reduced exposure to eavesdroppers. While the transmit area consistently outperforms the reflect area in the low-to-medium power range due to favorable power allocation and propagation conditions, the performance gap narrows as the power increases. This suggests that under high power conditions, the reflect area will begin to show improvements in secrecy performance that reduce the dominance of the transmit area. Therefore, increasing  $\rho$  allocates more power to the reflect area, that will increase  $R_r^{sec}$  and reduce  $R_t^{sec}$ , especially at higher power levels.

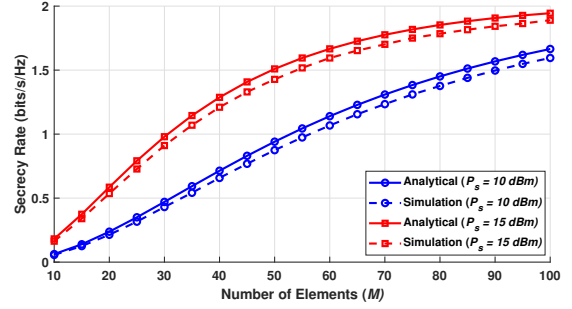


Figure 4. The secrecy rate versus the number of the elements  $M$  for the transmit area with different transmit power values.

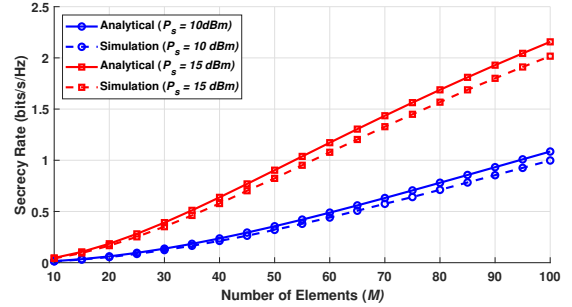


Figure 5. The secrecy rate versus the number of the elements  $M$  for the reflect area with different transmit power values.

In Fig. 4,  $R_t^{sec}$  is analyzed as a function of the number of RIS elements  $M$  at specific transmit power levels of 10 dBm, 15 dBm. The results indicate a clear relationship where increasing the number of RIS elements leads to substantial enhancements in achievable secrecy rates. For instance, as  $M$  increases from 10 to 100, the secrecy rate significantly improves, particularly at higher power levels. It also apparent that the Monte Carlo simulations validate the analytical curves, underscoring the effectiveness of deploying additional RIS elements to boost the system's secrecy capacity.

Similarly, Fig. 5 presents the secrecy rate performance in the reflect area  $R_r^{sec}$  concerning different values of  $M$  with the same transmit power levels. The trends observed indicate a more gradual increase in secrecy rates compared to the transmit area. While the increase is significant, it is not as pronounced as in the transmit area. This analysis confirms that increasing the number of RIS elements can significantly enhance PLS, even in the reflect area, albeit at a slower rate.

To maximize the total weighted secrecy rate in the proposed UAV-mounted STAR-RIS-assisted NOMA system, we first investigate the impact of the power-splitting ratio  $\zeta$ . The optimization process is carried out using Algorithm 2, which iteratively searches for the value of  $\zeta$  that yields the highest total weighted secrecy rate under the given system configuration.

As depicted in Fig. 6, the WSSR initially increases with  $\zeta$ , reaching its maximum at  $\zeta^* = 0.15$ . Beyond this point, further increases in  $\zeta$  lead to a slight degradation in performance, attributed to the imbalance between reflection and transmission

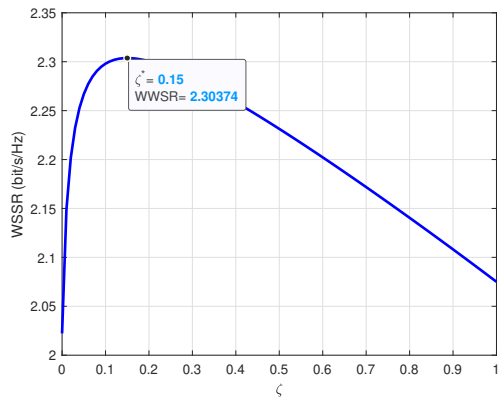


Figure 6. WSSR as a function of energy allocation ratio  $\zeta$  in the STAR-RIS-assisted system.

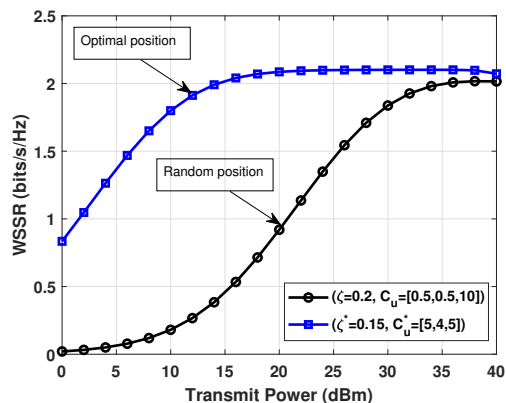


Figure 7. WSSR versus transmit power under a biased fairness scenario  $w_1 < w_2$ .

energy allocation in the STAR-RIS structure. Thus,  $\zeta^* = 0.15$  is selected as the optimal value for the subsequent evaluations.

Therefore, to evaluate the system's secrecy performance under different fairness strategies, the WSSR is evaluated as a function of the transmit power under two distinct weighting configurations. As shown in Fig. 7, the WSSR is evaluated under a biased fairness scenario where  $w_1 = 0.45$  and  $w_2 = 0.55$ , favoring the strong user. As observed, this configuration yields a higher WSSR across the transmit power range, particularly in the high-power regime, due to the stronger user's channel conditions being given more weight in the optimization process.

In contrast, Fig. 8 illustrates the performance under an equal fairness setting, with  $w_1 = w_2 = 0.5$ . Although the overall WSSR is slightly lower compared to the biased configuration, this setup ensures a more balanced secrecy performance between the two users, which is desirable in fairness-constrained scenarios. For both scenarios, the system parameters are  $M = 20$ ,  $k = 20$  and  $\rho = 0.3$ .

## VI. CONCLUSION

In this work, we presented a UAV-mounted STAR-RIS-assisted NOMA system for secure downlink communication in

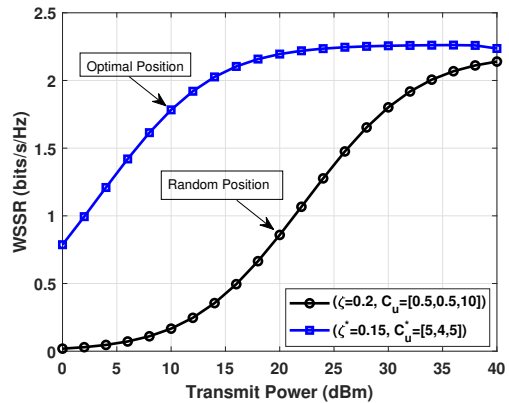


Figure 8. Total secrecy rate versus transmit power under an equal fairness scenario  $w_1 = w_2$ .

the presence of passive eavesdroppers. By modeling the phase estimation error using a von Mises distribution and approximating the composite angular error with a wrapped normal distribution, we derived accurate closed-form expressions for the ergodic secrecy rates in both reflection and transmission regions. Results show that the proposed analytical expressions closely match the Monte Carlo simulations, validating their accuracy and computational efficiency. In addition, the results demonstrate that the joint optimization of UAV placement and STAR-RIS power splitting significantly enhances secrecy performance, especially under high transmit power. Moreover, the findings reveal that phase estimation errors due to UAV mobility introduce noticeable degradation, and it was also shown that increasing the number of STAR-RIS elements improves secrecy but with diminishing returns. Finally, the optimal configuration is achieved when the power-splitting ratio and UAV location are jointly tuned, yielding the maximum total secrecy rate in our considered system.

These insights not only validate the robustness of the proposed model but also pave the way for the practical deployment of STAR-RIS-assisted UAV NOMA systems in next-generation secure wireless networks.

## APPENDIX A

The  $M$  complex variables  $|g_r| |h| e^{j\phi}$ ,  $m=1, \dots, M$ , are i.i.d. with common mean  $\mu = \alpha_r^2 \varphi_1$ , variance  $v = 1 - \alpha^4 |\varphi_1^2|$ , and pseudo-variance  $\rho = \varphi_2 - \alpha^4 \varphi_1^2$  (see [44] for the second-order characterization of complex variables).

According to the assumptions on the distribution of  $\phi$ , the trigonometric moments  $\varphi_1, \varphi_2 \in \mathbb{R}$  and, consequently  $\mu, \rho \in \mathbb{R}$ . By invoking the central limit theorem, we approximate the distribution of  $\sqrt{X}$  for  $M$  large by a complex normal distribution  $\mathcal{CN}(\mu, v/n, \rho/n)$ . Let  $U = \Re(H)$  and  $V = \Im(H)$ . Based on [45], we have

$$\text{Cov}[U, V] = \frac{1}{2} \Im\left(-\frac{v}{n} + \frac{\rho}{n}\right) = 0. \quad (42)$$

Being jointly Gaussian with zero covariance, it follows that  $U$  and  $V$  are independent. Furthermore,  $U \sim \mathcal{N}(\mu, \sigma_U^2)$ ,  $V \sim \mathcal{N}(0, \sigma_V^2)$  and  $\mu = \alpha^2 \varphi_1$

$$\sigma_U^2 = \frac{1}{2} \Re\left(\frac{v}{n} + \frac{\rho}{n}\right) = \frac{1}{2n}(1 + \varphi_2 - 2\alpha^4 \varphi_1^2), \quad (43)$$

$$\sigma_V^2 = \frac{1}{2} \Re\left(\frac{v}{n} - \frac{\rho}{n}\right) = \frac{1}{2n}(1 - \varphi_2). \quad (44)$$

## APPENDIX B

We consider the random variable  $X = U^2 + V^2$ , where the normalized variable  $U^2/\sigma_U^2$  follows a non-central chi-squared distribution, and  $V^2$  is Gamma distributed with shape parameter  $1/2$  and scale parameter  $2\sigma_V^2$ . Consequently,  $|H|^2$  can be expressed as the sum of a scaled non-central chi-squared variable and a Gamma variable. To characterize the distribution of  $X$  we utilize its cumulative generating function, defined as  $K_X(t) = \ln \mathbb{E}[e^{tX}]$ . Since  $U$  and  $V$  are independent (APPENDIX A)

$$\begin{aligned} K_X(t) &= K_{U^2}(t) + K_{V^2}(t), \\ &= \frac{\mu^2 t}{1 - 2\sigma_U^2 t} - \frac{1}{2} \ln(1 - 2\sigma_U^2 t) - \frac{1}{2} \ln(1 - 2\sigma_V^2 t). \end{aligned} \quad (45)$$

We now approximate for large  $M$  the first term in the r.h.s. We develop its Maclaurin series expansion as

$$\begin{aligned} \frac{\mu^2 t}{1 - 2\sigma_U^2 t} &= \mu^2 t + \mu^2 (2\sigma_U^2) t^2 + \mu^2 (2\sigma_U^2) t^3 + \dots \\ &= \frac{\mu^2}{4\sigma_U^2} \sum_{k=1}^{\infty} \frac{k}{2^{k-1}} \frac{(4\sigma_U^2 t)^k}{k} \\ &= \frac{\mu^2}{4\sigma_U^2} \sum_{k=1}^{\infty} \frac{(4\sigma_U^2 t)^k}{k} - g(t) \sum_{k=1}^{\infty} \frac{(4\sigma_U^2 t)^k}{k} \\ &= -\ln(1 - 4\sigma_U^2 t), \end{aligned} \quad (46)$$

where

$$\begin{aligned} g(t) &= \frac{\mu^2}{4\sigma_U^2} \sum_{k=3}^{\infty} \left(1 - \frac{k}{2^{k-1}}\right) \frac{(4\sigma_U^2 t)^k}{k} < \frac{\mu^2}{4\sigma_U^2} \sum_{k=3}^{\infty} \frac{(4\sigma_U^2 t)^k}{k} \\ &= 4\mu^2 \sigma_U^2 t^2 \sum_{k=1}^{\infty} \frac{(4\sigma_U^2 t)^k}{k+2} < 4\mu^2 \sigma_U^2 t^2 \sum_{k=1}^{\infty} \frac{(4\sigma_U^2 t)^k}{k} \\ &= -4\mu^2 \sigma_U^2 t^2 \ln(1 - 4\sigma_U^2 t). \end{aligned} \quad (47)$$

Given that  $\sigma_U^2 = O(M^{-1})$ , we have  $g(t) = O(M^{-2})$ , such that (45) is well approximated by

$$K_X(t) = -\frac{\mu^2}{4\sigma_U^2} \ln(1 - 4\sigma_U^2 t) - \frac{1}{2} \ln(1 - 2\sigma_U^2 t) - \frac{1}{2} \ln(1 - 2\sigma_V^2 t). \quad (48)$$

The expression (48) corresponds to the cumulative generating function of the sum of three independent Gamma variables with (shape, scale) parameters  $(\frac{\mu^2}{4\sigma_U^2}, 4\sigma_U^2)$ ,  $(1/2, 2\sigma_U^2)$ , and  $(1/2, 2\sigma_V^2)$ , respectively. While the resulting distribution can be characterized based on [45], we simplify by making a further approximation

$$K_X(t) = -\frac{\mu^2}{4\sigma_U^2} \ln(1 - 4\sigma_U^2 t), \quad (49)$$

which has  $O(M^{-1})$  error. Thus, for large  $M$ ,  $X$  has a Gamma distribution with shape  $\frac{\mu^2}{4\sigma_U^2}$  and scale  $4\sigma_U^2$ . It follows through variable transformation that  $\sqrt{X}$  has a Nakagami distribution with fading parameter (shape) and spread  $\mu^2$ . Therefore,

$$m = -\frac{\mu^2}{4\sigma_U^2} = \frac{M}{2} \frac{\varphi_1^2 \alpha^4}{1 + \varphi_2 - 2\varphi_1^2 \alpha^4}. \quad (50)$$

## ACKNOWLEDGMENT

This work was supported and funded by the Deanship of Scientific Research at Imam Mohammad Ibn Saud Islamic University (IMSIU) (grant number: IMSIU-DDRSP2504).

## REFERENCES

- [1] R. Alghamdi, R. Alhadrami, D. Alhathali, H. Almorad, A. Faisal, S. Helal, R. Shalabi, R. Asfour, N. Hammad, A. Shams, N. Saeed, H. Dahrouj, T. Y. Al-Naffouri, and M.-S. Alouini, "Intelligent surfaces for 6G wireless networks: A survey of optimization and performance analysis techniques," *IEEE Access*, vol. 8, pp. 202 795–202 818, 2020.
- [2] E. Arslan, F. Kilinc, S. Arzykulov, A. T. Dogukan, A. Celik, E. Basar, and A. M. Eltawil, "Reconfigurable intelligent surface enabled over-the-air uplink NOMA," *IEEE Trans. Green Commun. Netw.*, vol. 7, no. 2, pp. 814–826, 2023.
- [3] M. Najafi, V. Jamali, R. Schober, and H. V. Poor, "Physics-based modeling and scalable optimization of large intelligent reflecting surfaces," *IEEE Trans. Commun.*, vol. 69, no. 4, pp. 2673–2691, 2021.
- [4] F. Zhou, Z. Li, J. Cheng, Q. Li, and J. Si, "Robust an-aided beamforming and power splitting design for secure MISO cognitive radio with SWIPT," *IEEE Trans. Wireless Commun.*, vol. 16, no. 4, pp. 2450–2464, 2017.
- [5] X. Zhang, X. Zhou, and M. R. McKay, "Enhancing secrecy with multi-antenna transmission in wireless Ad Hoc networks," *IEEE Trans. Inf. Forensics Security*, vol. 8, no. 11, pp. 1802–1814, 2013.
- [6] Y. Liu, X. Liu, X. Mu, T. Hou, J. Xu, M. Di Renzo, and N. Al-Dhahir, "Reconfigurable intelligent surfaces: Principles and opportunities," *IEEE Commun. Surv. Tutor.*, vol. 23, no. 3, pp. 1546–1577, 2021.
- [7] Y. Liu, X. Mu, J. Xu, R. Schober, Y. Hao, H. V. Poor, and L. Hanzo, "STAR: Simultaneous transmission and reflection for 360° coverage by intelligent surfaces," *IEEE Wireless Commun.*, vol. 28, no. 6, pp. 102–109, 2021.
- [8] X. et al, "Simultaneous realization of anomalous reflection and transmission at two frequencies using bi-functional metasurfaces," *Sci.Reps.*, vol. 8, no. 1, pp. 1–8, 2018.
- [9] T. Wang, F. Fang, and Z. Ding, "An SCA and relaxation based energy efficiency optimization for multi-user RIS-assisted NOMA networks," *IEEE Trans. Veh. Technol.*, vol. 71, no. 6, pp. 6843–6847, 2022.
- [10] J. Chen, Z. Ma, Y. Zou, J. Jia, and X. Wang, "DRL-based energy efficient resource allocation for STAR-RIS assisted coordinated multi-cell networks," in *IEEE Global Commun. Conf. (GLOBECOM)*, 2022, pp. 4232–4237.
- [11] J. Chen, Y. Xie, X. Mu, J. Jia, Y. Liu, and X. Wang, "Energy efficient resource allocation for IRS assisted CoMP systems," *IEEE Trans. Wireless Commun.*, vol. 21, no. 7, pp. 5688–5702, 2022.
- [12] J. Chen, L. Guo, J. Jia, J. Shang, and X. Wang, "Resource allocation for IRS assisted SGF NOMA transmission: A MADRL approach," *IEEE J. Sel. Areas Commun.*, vol. 40, no. 4, pp. 1302–1316, 2022.
- [13] X. Mu, Y. Liu, L. Guo, J. Lin, and H. V. Poor, "Intelligent reflecting surface enhanced multi-UAV NOMA networks," *IEEE J. Sel. Areas Commun.*, vol. 39, no. 10, pp. 3051–3066, 2021.
- [14] J. Zhao, Y. Zhu, X. Mu, K. Cai, Y. Liu, and L. Hanzo, "Simultaneously transmitting and reflecting reconfigurable intelligent surface(STAR-RIS) assisted UAV communications," *IEEE J. Sel. Areas Commun.*, vol. 40, no. 10, pp. 3041–3056, 2022.
- [15] D. Liu, Y. Xu, J. Wang, J. Chen, K. Yao, Q. Wu, and A. Anpalagan, "Opportunistic UAV utilization in wireless networks: Motivations, applications, and challenges," *IEEE Commun. Mag.*, vol. 58, no. 5, pp. 62–68, 2020.

- [16] Z. Xiao, L. Zhu, Y. Liu, P. Yi, R. Zhang, X.-G. Xia, and R. Schober, "A survey on millimeter-wave beamforming enabled UAV communications and networking," *IEEE Commun. Surv. Tutor.*, vol. 24, no. 1, pp. 557–610, 2022.
- [17] Y.-S. Shiu, S. Y. Chang, H.-C. Wu, S. C.-H. Huang, and H.-H. Chen, "Physical layer security in wireless networks: a tutorial," *IEEE Wireless Commun.*, vol. 18, no. 2, pp. 66–74, 2011.
- [18] Z. Wei, Y. Cai, Z. Sun, D. W. Kwan Ng, and J. Yuan, "Sum-rate maximization for IRS-assisted UAV OFDMA communication systems," in *IEEE Global Commun. Conf. (GLOBECOM)*, 2020, pp. 1–7.
- [19] L. Ge, P. Dong, H. Zhang, J.-B. Wang, and X. You, "Joint beamforming and trajectory optimization for intelligent reflecting surfaces-assisted UAV communications," *IEEE Access*, vol. 8, pp. 78 702–78 712, 2020.
- [20] D. Tyrovolas, P.-V. Mekikis, S. A. Tegos, P. D. Diamantoulakis, C. K. Liaskos, and G. K. Karagiannidis, "Energy-aware design of UAV-mounted RIS networks for IoT data collection," *IEEE Trans. Commun.*, vol. 71, no. 2, pp. 1168–1178, 2023.
- [21] N. Wang, P. Wang, A. Alipour-Fanid, L. Jiao, and K. Zeng, "Physical-layer security of 5G wireless networks for IoT: Challenges and opportunities," *IEEE Internet Things J.*, vol. 6, no. 5, pp. 8169–8181, 2019.
- [22] X. Tang, D. Wang, R. Zhang, Z. Chu, and Z. Han, "Jamming mitigation via aerial reconfigurable intelligent surface: Passive beamforming and deployment optimization," *IEEE Trans. Veh. Technol.*, vol. 70, no. 6, pp. 6232–6237, 2021.
- [23] H. Guo, Y.-C. Liang, and S. Xiao, "Intelligent reflecting surface configuration with historical channel observations," *IEEE Wireless Commun. Lett.*, vol. 9, no. 11, pp. 1821–1824, 2020.
- [24] Q. Wu and R. Zhang, "Intelligent reflecting surface enhanced wireless network via joint active and passive beamforming," *IEEE Trans. Wireless Commun.*, vol. 18, no. 11, pp. 5394–5409, 2019.
- [25] Z. Chu, W. Hao, P. Xiao, and J. Shi, "Intelligent reflecting surface aided multi-antenna secure transmission," *IEEE Wireless Commun. Lett.*, vol. 9, no. 1, pp. 108–112, 2020.
- [26] S. Arzykulov, A. Celik, G. Nauryzbayev, and A. M. Eltawil, "Artificial noise and RIS-aided physical layer security: Optimal RIS partitioning and power control," *IEEE Wireless Commun. Lett.*, vol. 12, no. 6, pp. 992–996, 2023.
- [27] M. H. Khoshafa, T. M. N. Ngatched, and M. H. Ahmed, "Reconfigurable intelligent surfaces-aided physical layer security enhancement in D2D underlay communications," *IEEE Commun. Lett.*, vol. 25, no. 5, pp. 1443–1447, 2021.
- [28] Y. Zhang, S. Zhao, Y. Shen, X. Jiang, and N. Shiratori, "Enhancing the physical layer security of two-way relay systems with RIS and beamforming," *IEEE Trans. Inf. Forensics Security*, vol. 19, pp. 5696–5711, 2024.
- [29] J. Qiao and M.-S. Alouini, "Secure transmission for intelligent reflecting surface-assisted mmwave and Terahertz systems," *IEEE Wireless Commun. Lett.*, vol. 9, no. 10, pp. 1743–1747, 2020.
- [30] G. Zhou, C. Pan, H. Ren, K. Wang, and Z. Peng, "Secure wireless communication in RIS-aided MISO system with hardware impairments," *IEEE Wireless Commun. Lett.*, vol. 10, no. 6, pp. 1309–1313, 2021.
- [31] X. Yu, D. Xu, Y. Sun, D. W. K. Ng, and R. Schober, "Robust and secure wireless communications via intelligent reflecting surfaces," *IEEE J. Sel. Areas Commun.*, vol. 38, no. 11, pp. 2637–2652, 2020.
- [32] S. Hong, C. Pan, H. Ren, K. Wang, and A. Nallanathan, "Artificial-noise-aided secure MIMO wireless communications via intelligent reflecting surface," *IEEE Trans. Commun.*, vol. 68, no. 12, pp. 7851–7866, 2020.
- [33] J. Zhao, Y. Zhu, X. Mu, K. Cai, Y. Liu, and L. Hanzo, "Simultaneously transmitting and reflecting reconfigurable intelligent surface (STAR-RIS) assisted UAV communications," *IEEE J. Sel. Areas Commun.*, vol. 40, no. 10, pp. 3041–3056, 2022.
- [34] B. Zheng and R. Zhang, "IRS meets relaying: Joint resource allocation and passive beamforming optimization," *IEEE Wireless Commun. Lett.*, vol. 10, no. 9, pp. 2080–2084, 2021.
- [35] C. Wu, Y. Liu, X. Mu, X. Gu, and O. A. Dobre, "Coverage characterization of STAR-RIS networks: NOMA and OMA," *IEEE Commun. Lett.*, vol. 25, no. 9, pp. 3036–3040, 2021.
- [36] X. Mu, Y. Liu, L. Guo, J. Lin, and R. Schober, "Simultaneously transmitting and reflecting (STAR) RIS aided wireless communications," *IEEE Trans. Wireless Commun.*, vol. 21, no. 5, pp. 3083–3098, 2022.
- [37] J. Xu, Y. Zeng, and R. Zhang, "UAV-enabled wireless power transfer: Trajectory design and energy optimization," *IEEE Trans. Wireless Commun.*, vol. 17, no. 8, pp. 5092–5106, 2018.
- [38] Z. Ding, Y. Liu, J. Choi, Q. Sun, M. Elkashlan, I. Chih-Lin, and H. V. Poor, "Application of non-orthogonal multiple access in LTE and 5G networks," *IEEE Commun. Mag.*, vol. 55, no. 2, pp. 185–191, 2017.
- [39] X. Mu, Y. Liu, L. Guo, J. Lin, and R. Schober, "Simultaneously transmitting and reflecting (STAR) RIS aided wireless communications," *IEEE Trans. Wireless Commun.*, vol. 21, no. 5, pp. 3083–3098, 2022.
- [40] J. Yao, J. Xu, W. Xu, D. W. K. Ng, C. Yuen, and X. You, "Robust beamforming design for RIS-aided cell-free systems with CSI uncertainties and capacity-limited backhaul," *IEEE Trans. Commun.*, vol. 71, no. 8, pp. 4636–4649, 2023.
- [41] G. Zhang, Q. Wu, M. Cui, and R. Zhang, "Securing UAV communications via joint trajectory and power control," *IEEE Trans. Wireless Commun.*, vol. 18, no. 2, pp. 1376–1389, 2019.
- [42] J. D. Vega Sánchez, P. Ramírez-Espinosa, and F. J. López-Martínez, "Physical layer security of large reflecting surface aided communications with phase errors," *IEEE Wireless Commun. Lett.*, vol. 10, no. 2, pp. 325–329, 2021.
- [43] K. A. Hamdi, "A useful lemma for capacity analysis of fading interference channels," *IEEE Trans. Commun.*, vol. 58, no. 2, pp. 411–416, 2010.
- [44] B. Picinbono, "Second-order complex random vectors and normal distributions," *IEEE Trans. Signal Process.*, vol. 44, no. 10, pp. 2637–2640, 1996.
- [45] P. G. Moschopoulos, "The distribution of the sum of independent Gamma random variables," *Ann. Inst. Stat. Math.*, vol. 37, no. 3, p. 541–544, 1985.